Optical Characterization of $NaBi(MoO_4)_2$ Crystal by Spectroscopic Ellipsometry

I. Guler[a], M. Isik[b], N.M. Gasanly[c,d]

[a]*Physics, Inter-Curricular Courses Department, Çankaya University, 06530 Ankara, Turkey*
[b]*Department of Electrical and Electronics Engineering, Atilim University, 06836 Ankara, Turkey*
[c]*Department of Physics, Middle East Technical University, 06800 Ankara, Turkey*
[d]*Virtual International Scientific Research Centre, Baku State University, 1148 Baku, Azerbaijan*

Abstract

The compound $NaBi(MoO_4)_2$ has garnered significant interest in optoelectronic fields. This study employs spectroscopic ellipsometry to thoroughly examine the linear and nonlinear optical characteristics of $NaBi(MoO_4)_2$ crystals, offering detailed insights into their optical behavior. Our investigation presents a precise method for discerning the crystal's spectral features, revealing the spectral variations of key optical parameters such as refractive index, extinction coefficient, dielectric function, and absorption coefficient within the 1.2-5.0 eV range. Through analysis, we determined optical attributes including bandgap energy, critical point energy, and single oscillator parameters. Additionally, we explored the nonlinear optical properties of $NaBi(MoO_4)_2$, unveiling potential applications such as optoelectronic devices, frequency conversion, and optical sensors. This study enhances comprehension of optical properties of $NaBi(MoO_4)_2$, underscoring its significance in future optical and electronic advancements.

Keywords: Double tungstates, $NaBi(WO_4)_2$, $NaBi(MoO_4)_2$, optical properties, ellipsometry

Published by APPLIED PHYSICS A-MATERIALS SCIENCE & PROCESSING
https://doi.org/10.1007/s00339-024-07771-6

1. Introduction

$NaBi(MoO_4)_2$, also known as sodium bismuth molybdate, is a compound belonging to the family of molybdate-based materials. The crystal structure of $NaBi(MoO_4)_2$ is characterized by a three-dimensional network composed of corner-sharing MoO_4 tetrahedra and BiO_6 octahedra, with sodium ions occupying the interstitial sites within this framework [1]. This unique arrangement offers opportunities for ion exchange and intercalation processes, contributing to its functionality in different applications. $NaBi(MoO_4)_2$ exhibits interesting optical properties, making it a potential candidate for various applications such as optoelectronics, luminescent materials, and photovoltaics [2]. $NaBi(MoO_4)_2$ displays intriguing characteristics including elevated ionic conductivity, favorable chemical durability, and catalytic potential, rendering it a viable candidate for application in electrochemical apparatus, solid oxide fuel cells, and sensor technology. These properties make it valuable for various applications in materials science and technology. In recent years, $NaBi(MoO_4)_2$ has been investigated for its potential applications in fields such as energy storage, electrocatalysis, photocatalysis, and environmental remediation. For instance, it has shown promise as a solid electrolyte in solid oxide fuel cells due to its high ionic conductivity. Additionally, its catalytic activity has been explored for applications in water splitting, CO_2 reduction, and organic transformations [3-5]. $NaBi(MoO_4)_2$ has also been studied extensively for its luminescent properties, particularly in the field of solid-state lighting and display technologies [6]. Its ability to emit light under certain conditions makes it suitable for use in phosphors and light-emitting diodes (LEDs) [7]. Moreover, $NaBi(MoO_4)_2$ has been investigated for its potential applications in photocatalysis and solar energy conversion due to its ability to absorb light in the visible region [8].

The crystal structure of $NaBi(MoO_4)_2$ belongs to the monoclinic crystal system. It crystallizes in the space group P21/c with the following lattice parameters: a = 13.215 Å, b = 7.082 Å, c = 7.357 Å, and β = 111.12°. The structure consists of $[BiMoO_6]$ and $[NaO_6]$ octahedra, where each sodium cation is coordinated by six oxygen atoms, forming distorted octahedra. The bismuth and molybdenum atoms are also coordinated by oxygen atoms, forming distorted octahedral units. These units are interconnected through corner-sharing oxygen atoms, resulting in the formation of a three-dimensional framework structure [9,10].

The fundamental aspects of semiconductor technology are significantly impacted by optical parameters like refractive index, band energy, extinction coefficient, and absorption coefficient. Precise identification of these factors is crucial for enhancing the efficiency and

functionality of semiconductor devices through improved design, production, and performance optimization. Given the significance of this aspect, this paper employs for the first time ellipsometry investigation to acquire spectral dependencies for different optical characteristics of the $NaBi(MoO_4)_2$ crystal. The analysis of ellipsometry data, employing an appropriate optical model, enables the determination of band energy, single oscillator parameters, and nonlinear optical properties based on the obtained spectral distributions of the optical parameters.

2. Experimental details

$NaBi(MoO_4)_2$ crystals were synthesized via the Czochralski method and then subjected to a 800°C heat treatment for 24 hours to achieve a single-phase outcome. The crystal growth process utilized a pulling rate of 2 mm/h and a rotation rate of 15 rpm, resulting in elongated crystals. These crystals were subsequently cut and polished, yielding $NaBi(MoO_4)_2$ crystals measuring $1.5 \times 1.2 \times 0.1$ cm^3 with excellent optical quality. The photo of the crystal obtained after growth and subsequent cutting processes was given in our previously published article [11]. The grown bulk crystal exhibited good transparent optical properties. In addition, in the same reference article, x-ray diffraction (XRD) measurements were carried out to examine the structural properties of the crystal, and the XRD pattern showed that the grown crystal has high quality crystallinity. The peaks observed in the XRD pattern also indicated that the crystal had tetragonal crystal structure. Spectroscopic ellipsometry measurements were performed at room temperature using a SOPRA GES-5E ellipsometer equipped with a rotating polarizer, covering a spectral range from 1.2 to 5.0 eV with 0.01 eV increments, and directed towards the crystal surface at a 70-degree angle.

3. Results and discussions

Ellipsometry measurements were utilized to analyze the optical properties of $NaBi(MoO_4)_2$ single crystal across an energy spectrum from 1.2 to 5.0 electronvolts (eV). This method involves directing a linearly polarized beam onto the sample and then extracting experimental data from the amplitude ratio (Ψ) and phase shift (Δ) of both parallel (p) and perpendicular (s) components of the reflected light [12]. Figure 1 illustrates the spectral variations of Ψ and Δ parameters.

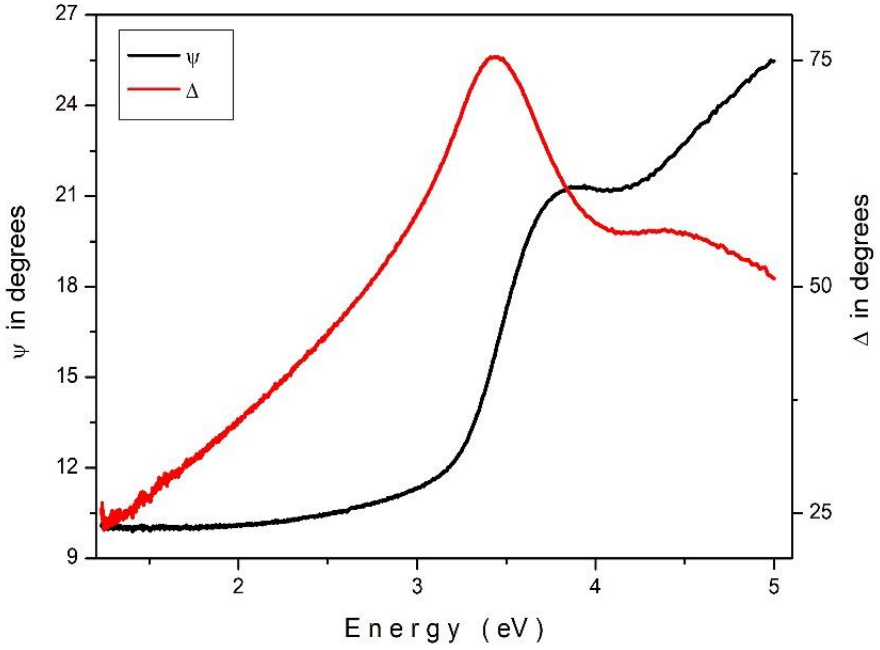

Figure 1. Spectra of amplitude ratio and phase shift.

Analyzing Ψ and Δ involves creating a suitable theoretical framework derived from the structural properties of the sample under investigation. In the context of bulk crystals, the established optical model can be represented by the subsequent equation, which depicts the interaction between air and the sample [13]

$$\varepsilon = \varepsilon_1 + i\varepsilon_2 = \sin^2(\varphi)\left[1 + \left(\frac{1-\rho}{1+\rho}\right)^2 \tan^2(\varphi)\right], \quad (1)$$

where $\rho = \tan\Psi \exp(i\Delta)$. In the equation, φ represents the angle of incidence, while ε_1 and ε_2 denote the real and imaginary components of the complex dielectric function, respectively. The spectra for ε_1 and ε_2, derived from the analysis of ellipsometry data presented in Figure 1 using Eq. (1), are illustrated in Figure 2. The ε_1 spectrum demonstrates typical dispersion behavior below the band gap energy, with values hovering around ~4.3. Based on this observation, the low-frequency dielectric constant, $\varepsilon_1(0)$, of the $NaBi(MoO_4)_2$ single crystal can be estimated to be approximately this value. The extinction coefficient rises with energy significantly in the 1.1-3.4 eV and slightly 4.1-4.3 eV ranges, a trend attributed to interband transitions within semiconductor materials. As photon energy increases, semiconductors facilitate electron promotion across their bandgaps. This phenomenon leads to heightened absorption coefficients and, consequently, increased extinction coefficients. Ellipsometer

investigations have noted that peaks in the extinction coefficient spectrum correspond to energy differences between relevant bands [14-16]. In the ε_2 spectrum, two peaks are discernible at energy levels around 3.47 and 4.35 eV. These energy values correspond to transitions between bands and are referred to as critical point energies in the dielectric function.

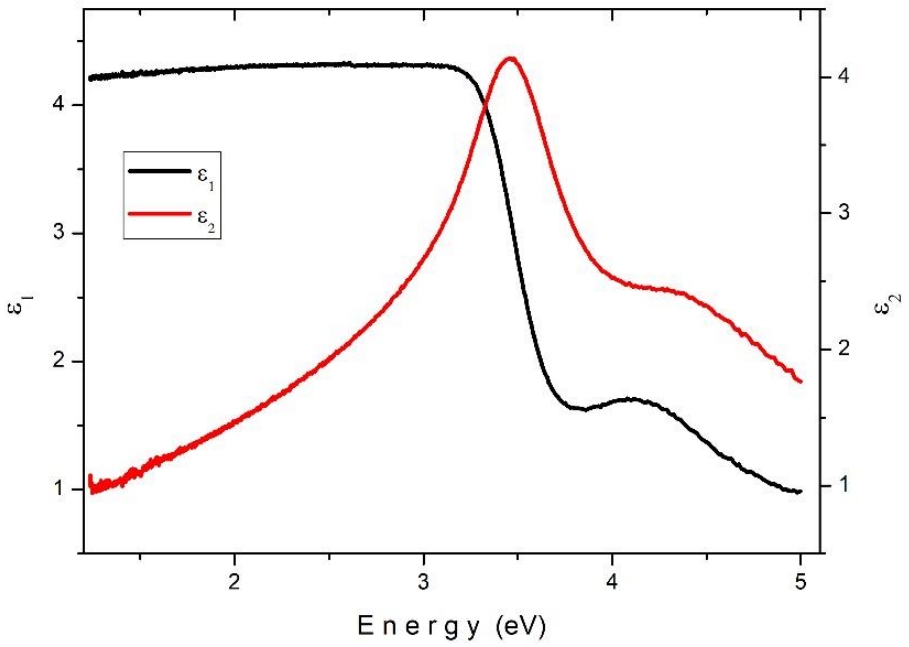

Figure 2. Spectra of real and imaginary parts of dielectric function for $NaBi(MoO_4)_2$.

To confirm this observation, we extensively examined the ε_2 spectrum using a method that calculates the second derivative of energy. This examination produced the $d^2\varepsilon_2/dE^2$ spectrum, displayed in Figure 3, covering energies from 2.85 to 4.70 eV. Following this analytical approach, a dip in the spectrum indicates an energy value linked to a significant absorption occurrence. Specifically, the $d^2\varepsilon_2/dE^2$ spectrum exhibits dips at approximately 3.46 and 4.37 eV, corresponding to critical points of the $NaBi(MoO_4)_2$ crystal.

.

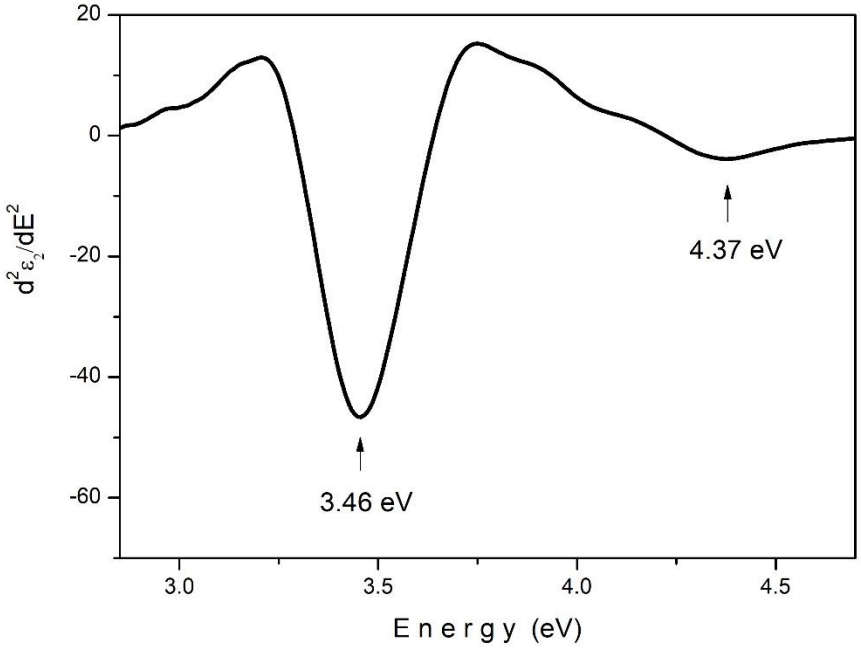

Figure 3. The spectral variation of the plot displaying the second derivative of ε_2 with respect to energy.

The relationship between the values of ε_1 and ε_2, which represent the elements of the dielectric function, and the refractive index (n) and extinction coefficient (k) values is described as follows [17]:

$$n = \left[\left(\varepsilon_1 + (\varepsilon_1^2 + \varepsilon_2^2)^{1/2}\right)/2\right]^{1/2} \quad (2)$$

$$k = \left[\left(-\varepsilon_1 + (\varepsilon_1^2 + \varepsilon_2^2)^{1/2}\right)/2\right]^{1/2} \quad (3)$$

The refractive index and extinction coefficient spectra obtained using the above formulas and spectra given in the Figure 2 are shown in Figure 4. The refractive index is around 2.1 below the band gap energy. Analysis of the current spectra shows that the refractive index decreases as energy levels rise. Conversely, the extinction coefficient increases with higher energy levels, suggesting increased light absorption, especially in the higher energy range. Therefore, this suggests that the material is more optically transparent at lower energy levels but absorbs more light at higher energy levels.

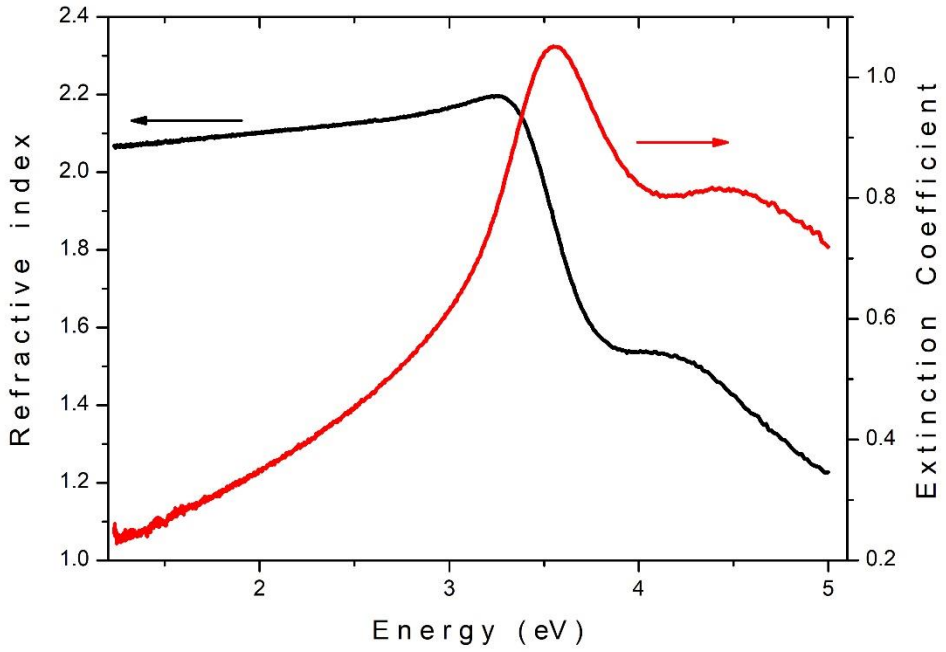

Figure 4. The refractive index and extinction coefficient spectra of the $NaBi(MoO_4)_2$ crystal.

The study below the absorption edge examined refractive index dispersion using the Wemple and DiDomenico single oscillator model. This model links the refractive index to the single oscillator (E_{so}) and dispersion energies (E_d), which are measures of the average energy bandgap and the intensity of interband optical transitions, respectively. The model's expression is as follows [18,19]:

$$n^2(h\nu) = 1 + \frac{E_{so}E_d}{E_{so}^2 - (h\nu)^2}. \quad (4)$$

By conducting a simple examination of Eq. (4), we produced a plot depicting $(n^2-1)^{-1}$ vs. $(h\nu)^2$, with emphasis on longer wavelengths to clarify E_{so} and E_d. The gradient of the linear regression applied to the data yields a value representing $1/E_{so}E_d$. The point where the fitted line intersects the vertical axis indicates the ratio of E_{so} to E_d. Figure 5 displays a plot of $(n^2-1)^{-1}$ vs. $(h\nu)^2$. Analysis using linear regression on the collected data resulted in a slope of 0.00576 and an intercept of 0.32257. By applying these values, we determined E_{so} and E_d of the $NaBi(MoO_4)_2$ crystal as 7.48 eV and 23.19 eV, respectively. Later on, we determined the static refractive index (n_0) and dielectric constant (ε_0) of the $NaBi(MoO_4)_2$ crystal using the formulas of $n_0 =$

$(1 + E_d/E_{so})^{1/2}$ and $\varepsilon_0 = n_0^2$, yielding values of n_0 = 2.02 and ε_0 = 4.1, respectively. The real part of the dielectric function is presented in the Spitzer-Fan model as follows [20, 21]:

$$\varepsilon_1 = n^2 - k^2 = \varepsilon_\infty - \left[\frac{e^2}{4\pi^2 C^2\ \varepsilon_0}\right]\left(\frac{N}{m^*}\right)\lambda^2 \qquad [5]$$

The symbol ε_∞ stands for the dielectric constant at high frequencies, independent of any influence from free carriers. In this context, *N* represents carrier concentration, *m** indicates effective mass, *C* denotes the speed of light, ε_o stands for the dielectric constant of free space and *e* corresponds to electronic charge. The inset in Figure 5 demonstrates the relationship between $n^2 - k^2$ and λ^2, allowing for the determination of ε_∞ and *N/m** by intersecting the plot with the $n^2 - k^2$ axis and determining the gradient of the linear regression, respectively. As a result, we calculated values of ε_∞ as 4.35 and *N/m** as 1.776×10^{47} g^{-1} cm^{-3}, respectively.

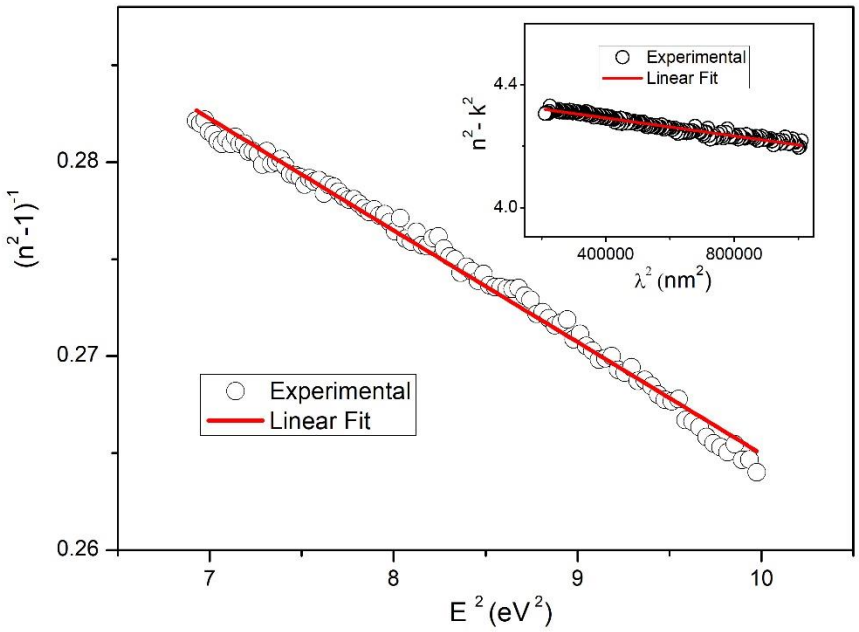

Figure 5. $(n^2-1)^{-1}$ vs. $(h\nu)^2$ plot for Wemple and DiDomenico single oscillator model. Inset: $n^2 - k^2$ vs. λ^2 plot for Spitzer-Fan model.

The connection between the absorption coefficient (α) and the extinction coefficient (k) is described by the commonly acknowledged equation $\alpha = 4\pi k/\lambda$, where λ (in nanometers) equals 1240 divided by *E*, with *E* denoting energy in electron volts (eV). In Figure 6, we have illustrated the spectral variation of α for the $NaBi(MoO_4)_2$ crystal, using data derived from the extinction coefficient spectrum. Determining the bandgap energy (E_g) primarily involves

analyzing α, owing to the well-established Tauc relationship between these two optical parameters, as referenced [17]

$$(\alpha hv) = A\big(hv - E_g\big)^p \tag{6}$$

The constant *A* remains constant regardless of energy variations, where " *hv* " represents the energy of electromagnetic radiation, and "*p*" takes values of 1/2 for direct transitions and 2 for indirect ones. Eq. (6), is utilized to extract the bandgap from a graphical depiction of $(\alpha hv)^{1/p}$ versus *hv* concerning photon energy. This correlation demonstrates a linear trend in the strong absorption area, and the line fitted linearly intersects the energy axis at the bandgap. The inset in Figure 6 illustrates the corresponding plot and the linear regression applied to it. The bandgap of the $NaBi(MoO_4)_2$ crystal was determined to be approximately 3.04 eV, corresponding to the point where the linear fit intersects the energy axis. This bandgap value, relatively high for semiconductor materials, presents opportunities for the $NaBi(MoO_4)_2$ crystal, particularly in LED design targeting the blue to UV light spectrum, in the manufacture of laser diodes for telecommunications, data storage, and medical applications, and in UV sensor development.

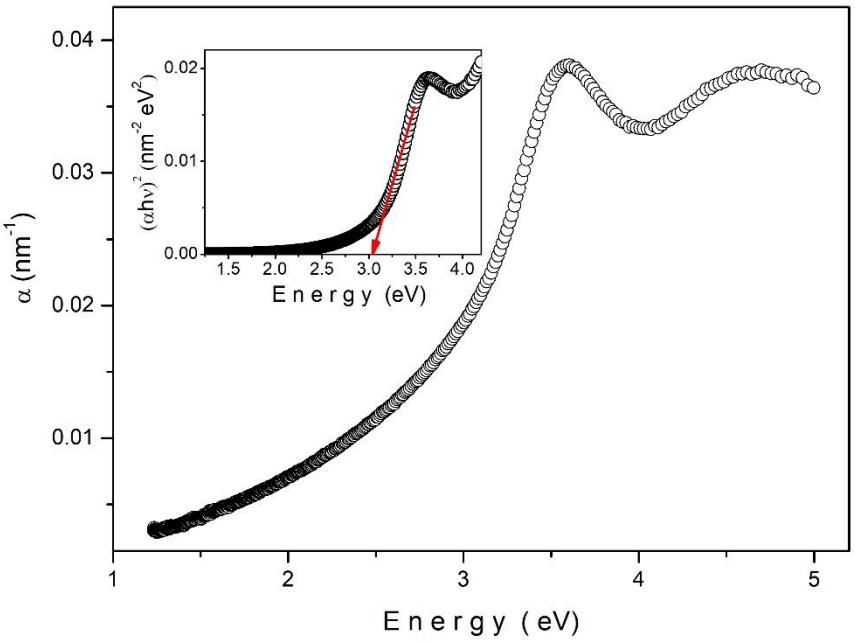

Figure 6. Variation in absorption coefficient with wavelength. The inset illustrates the graph used for Tauc analysis.

The intricate optical conductivity (σ_{op}) is represented by the subsequent equation [22,23]

$$\sigma_{op} = \sigma_1 + i\sigma_2 \quad (7)$$

The real and imaginary parts are expressed in relation to the vacuum permittivity (ε_0), angular frequency (ω), refractive index, and extinction coefficient as outlined below.

$$\sigma_1 = \omega\varepsilon_0\varepsilon_2 = 2nk\omega\varepsilon_0 \text{ and } \sigma_2 = \omega\varepsilon_0\varepsilon_1 = \omega\varepsilon_0(n^2 - k^2) \quad (8)$$

Using the *n*- and *k*-spectra, we produced spectral illustrations of the individual parts of the optical conductivity, illustrated in Figure 7. The actual part is strongly associated with energy dissipation happening within the substance. Notably, it becomes evident that there are increased energy dissipation at peak highest points, aligning with interband shifts happening at certain energy levels. Conversely, the imaginary part offers understanding into the likelihood of an electron within the substance absorbing a photon with a specific energy, resulting in a shift to a higher-energy state.

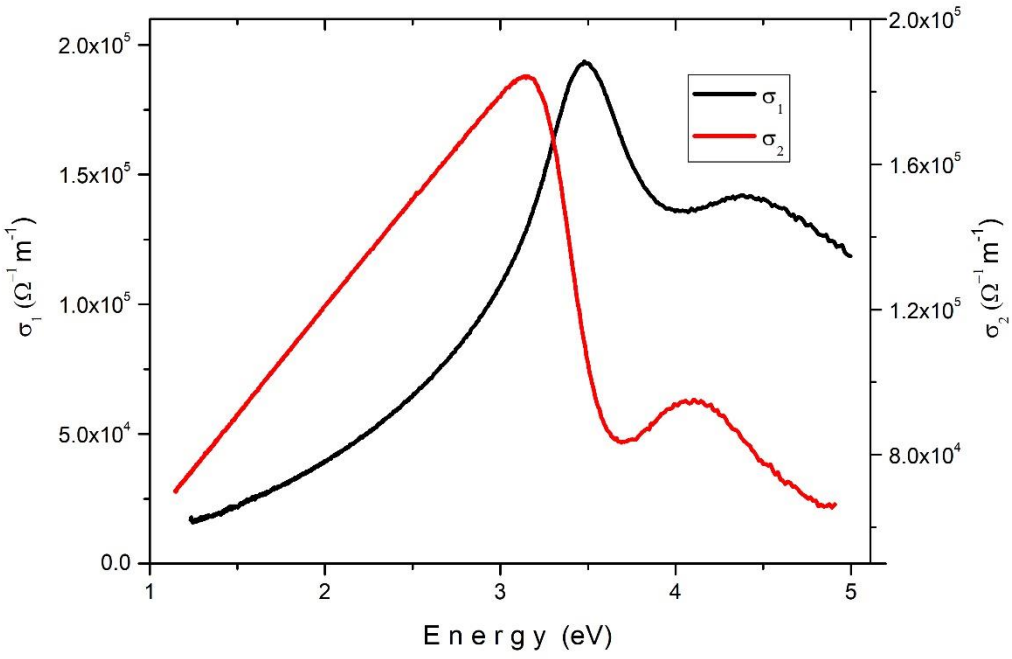

Figure 7. The optical conductivity spectra of $NaBi(MoO_4)_2$ crystal's real and imaginary components.

Assessing the nonlinear optical properties of semiconductor materials used in optoelectronic devices like optical switches, data storage, and signal processors is crucial. Therefore, we conducted an evaluation of the nonlinear optical characteristics of $NaBi(MoO_4)_2$ crystal. More precisely, we formulated equations for the nonlinear refractive index (n_2), first-order nonlinear susceptibility ($\chi^{(1)}$), and third-order nonlinear susceptibility ($\chi^{(3)}$) [24, 25]:

$$\chi^{(1)} = \frac{n_0^2-1}{4\pi}, \quad \chi^{(3)} = \frac{1.7\times10^{-10}}{(4\pi)^4}[n_0^2-1]^4 \quad \text{and} \quad n_2 = \frac{12\pi\chi^{(3)}}{n_0} \tag{9}$$

where n_0 was obtained from Wemple and DiDomenico analysis as 2.02. The nonlinear optical parameters were calculated as $\chi^{(1)}$ = 0.25 esu, $\chi^{(3)} = 6.2 \times 10^{-13}$ esu and $n_2 = 1.15 \times 10^{-11}$ esu. At this point, it will be useful to interpret the calculated nonlinear optical parameters and associate them with potential application areas. $NaBi(MoO_4)_2$ crystal exhibits many advantageous nonlinear optical properties. Firstly, its first-order nonlinear sensitivity value of $\chi^{(1)}$ = 0.25 esu indicates a remarkable responsiveness to external electric fields and registers the crystal as a suitable material for various nonlinear optical applications such as optical modulator [26, 27] and optical switching [28, 29]. The nonlinear optical parameters $\chi^{(3)} = 6.2 \times 10^{-13}$ esu and $n_2 = 1.15 \times 10^{-11}$ esu indicate the high capacity of the crystal for nonlinear optical operations. These values are higher than those observed in many other materials. This points to the potential of the $NaBi(MoO_4)_2$ crystal in nonlinear optical applications such as self-phase modulation, four-wave mixing [30], and optical switching [28, 29]. As a result, $NaBi(MoO_4)_2$ crystal exhibits superior nonlinear optical properties when compared to other materials, making it a promising candidate for the aforementioned applications.

4. Conclusion

In this paper, we conducted a thorough examination of the optical characteristics of the $NaBi(MoO_4)_2$ crystal within the 1.2-5.0 eV spectral range, offering valuable insights into its behavior and potential applications in optoelectronic devices. We presented the spectral variations of the crystal's refractive index, extinction coefficient, absorption coefficient, dielectric function, and optical conductivity function across the investigated energy spectrum. These alterations provide significant understanding of how the crystal interacts with incident light and its suitability for light manipulation. Through Tauc analysis, we determined the direct bandgap as 3.04 eV, suggesting promise for the $NaBi(MoO_4)_2$ crystal in optoelectronic devices operating in the blue to UV light range. Utilizing second derivative analysis of the dielectric function, we identified the critical point energies as 3.46 and 4.37 eV, a crucial parameter for elucidating electronic transitions within the crystal. Employing the Wemple and DiDomenico

single oscillator model, we derived the static refractive index and dielectric constant of the $NaBi(MoO_4)_2$ crystal as 2.02 and 4.10, respectively. Furthermore, we calculated the nonlinear refractive index, first-order nonlinear susceptibility, and third-order nonlinear susceptibility as 1.15×10^{-11} esu, 0.25, and 6.2×10^{-13} esu, respectively. These linear and nonlinear optical characteristics furnish valuable insights into the potential applications of the $NaBi(MoO_4)_2$ crystal in optoelectronic, nonlinear and photonic devices.

References:

[1] H. Wu, Y. Li, X. Wang, J. Solid State Chem. 183, 1103 (2010).

[2] J. C. Wu, S. Y. Chu, H. C. Kuo, J. Mater. Sci. Mater. Electron. 28, 5805 (2017).

[3] Q. Li, K. Huang, Z. Zhang, Q. Wu, F. Gao, MRX 7(9), 092001 (2020).

[4] S. Han, H. Zhang, MSEB 231, 60 (2018).

[5] L. Chen, Y. Zhang, J. Liu, J. Zou, Mater. Lett. 176, 81 (2016).

[6] J. Hao, S. M. Morris, A. M. Alshehri, J. Lumin. (2016) http://dx.doi.org/10.1016/j.jlumin.2016.04.039

[7] S. Zhang, Y. Wang, S. Feng, J. Alloys Compd. (2019) https://doi.org/10.1016/j.jallcom.2019.03.353

[8] Y. Song, L. Wu, J. Zhou, Mater. Lett. (2019) https://doi.org/10.1016/j.matlet.2018.11.042

[9] J.F. Li, X.L. Wang, S.B. Zhang, J.G. Zheng, Z.H. Zhang, G.Y. Yang, J. Alloys Compd. (2010) https://doi.org/10.1016/j.jallcom.2010.05.053

[10] L. Hamlaoui, S. Férid, R. Moreno, A. Ben Salah, J. Solid State Chem. (2016) http://dx.doi.org/10.1016/j.jssc.2016.01.015

[11] M. Isik, I. Guler, N.M. Gasanly, Phys. Scr. (2023) https://doi.org/10.1088/1402-4896/acb4c3

[12] Y. Wang, J. Lian, M. Wei, Y. Shi, K. Jin, C. Wang, Y. Zhang, Z. Xu, X. Zhou, Y. Li, Opt. Mater. (2022) https://doi.org/10.1016/j.optmat.2022.112727

[13] I. Guler, M. Isik, N.M. Gasanly, L.G. Gasanova, R.F. Babayeva, J. Electron. Mater. (2019) https://doi.org/10.1007/s11664-019-07000-4

[14] D.H. Li, H. Zheng, Z.Y. Wang, R.J. Zhang, H. Zhang, Y.X. Zheng, S.Y. Wang, D.W. Zhang, L.Y. Chen, Phys. Chem. Chem. Phys. (2017) https://doi.org/10.1039/C7CP00660H

[15] X. Zhu, J. He, R. Zhang, C. Cong, Y. Zheng, H. Zhang, S. Zhang, L. Chen, Nanoscale (2020) https://doi.org/10.1039/D0NR04591H

[16] I. Mohelský, A. Dubroka, J. Wyzula, A. Slobodeniuk, G. Martinez, Y. Krupko, B.A. Piot, O. Caha, J. Humlícek, G. Bauer, G. Springholz, M. Orlita, Phys. Rev. B (2020) https://doi.org/10.1103/PhysRevB.102.085201

[17] J.I. Pankove, Prentice-Hall, Englewood Cliffs, New Jersey, 1971.

[18] S.A. Khan, S. Patel, P. Shukla, R. Kumar, R. Dixit, Physica B (2023) https://doi.org/10.1016/j.physb.2023.414897

[19] A. Kompa, B.L. Devi, U. Chaitra, Mater. Chem. Phys. (2023) https://doi.org/10.1016/j.matchemphys.2023.127507

[20] E. Gnenna, N. Khemiri, M.I. Alonso, M. Kanzari, Optik (2022) https://doi.org/10.1016/j.ijleo.2022.169740

[21] A. B. Migdadi, A.A. Ahmad, A.M. Alsaad, A. Telfah, J. Mater. Sci. Mater. Electron. (2022) https://doi.org/10.1007/s10854-022-07699-8

[22] A. Qasem, M.S. Mostafa, H.A. Yakout, M. Mahmoud, E.R. Shaaban, Opt. Laser Technol. (2022) https://doi.org/10.15251/CL.2022.196.389

[23] D. Kim, Y. Jeon, J.L. MacManus-Driscoll, S. Lee, Adv. Funct. Mater. (2023) https://doi.org/10.1002/adfm.202300819

[24] A. Parida, D. Sahoo, D. Alagarasan, S. Vardhrajaperumal, R. Ganesan, R. Naik, Mater. Adv. (2022) https://doi.org/10.1039/D2MA00485B

[25] S. Das, S. Senapati, D. Alagarasan, R. Naik, Mat. Sci. Semicon. Proc. (2023) https://doi.org/10.1016/j.mssp.2023.107456

[26] A. Chizhikov, K. Yushkov, V. Molchanov, In Proceedings of the Fourteenth School on Acousto-Optics and Applications, Toruń, Poland, 2019.
https://doi.org/10.1117/12.2541046

[27] M.M. Mazur, A.A. Pavlyuk, A.V. Ryabinin, Inorg. Mater. (2021)
https://doi.org/10.1134/S0020168521040099

[28] B. Binish, K. Mani Rahulan, J. Photochem. Photobiol. A (2023)
https://doi.org/10.1016/j.jphotochem.2023.114614

[29] B. Binish, B. Lokesh, Y. Veer, S. Peters, M. Abith, T.C. Sabari Girisun, K. Mani Rahulan, Sci Rep (2024).
https://doi.org/10.1038/s41598-024-53690-0

[30] K. Koynov, P. Mitev, I. Buchvarov, S. Saltiel, Pure Appl. Opt. (1996)
https://doi.org/10.1088/0963-9659/5/1/010